Mechanical Systems and Signal Processing 211 (2024) 111181

Contents lists available at ScienceDirect

Mechanical Systems and Signal Processing

journal homepage: www.elsevier.com/locate/ymssp

Measurement and identification of the in-plane dynamic behaviour of a rolling tyre

Ivano La Paglia [a,*], Luca Rapino [a], Francesco Ripamonti [a], Simone Baro [b], Roberto Corradi [a]

[a] Politecnico di Milano, Department of Mechanical Engineering, Via La Masa 1, 20156 Milano, Italy
[b] Pirelli Tyre S.p.A., Viale Piero e Alberto Pirelli 25, 20126 Milano, Italy

ARTICLE INFO

Communicated by John E. Mottershead

Keywords:
Rolling tyre dynamics
Experimental cleat test
Wave propagation solution
Identification algorithm
Structure-borne noise

ABSTRACT

Road vehicle NVH performances can be improved acting on tyres, which play a fundamental role in the transmission of structure-borne noise and vibration into the cabin, up to 500 Hz. This paper aims at investigating the in-plane dynamics of a rolling tyre in this frequency range. Tyre radial vibration measurements are carried out through a dedicated experimental setup, based on a laser triangulation sensor scanning the tread of a rolling tyre. The experimental data are collected during cleat tests, considering different rolling speeds and inflation pressures, to investigate their influence on tyre dynamics. Then, a data processing algorithm is proposed with the aim of identifying the progressive and regressive waves propagating along the tyre circumference after the cleat impact. Finally, to interpret the results, the identified tyre response has been compared to the analytical results obtained through a simplified in-plane tyre model.

1. Introduction

The attention of the automotive industry to vehicle comfort is significantly increasing. As a result, the attention is posed to the improvement of the vehicle NVH (Noise, Vibration and Harshness) performances [1,2]. Moreover, in recent years electric vehicles are becoming more and more popular, so that tyre/road interaction is nowadays the most important contributor to the overall noise and vibration levels perceived in a vehicle [3]. In addition, the passengers' perception of the cabin is also changing due to the introduction of autonomous driving features. In this context, road vehicle NVH performances must be improved acting especially on tyres, which play a fundamental role in structure-borne cabin noise and vibration up to 500 Hz [4,5].

Different approaches can be adopted to investigate the dynamic behaviour of the tyre. On the one hand, from a modelling point of view, several solutions may be considered depending on the desired level of complexity. Analytical models are computationally efficient and provide results in a short time; however, they provide only a general understanding of the phenomenon [6]. Finite element models require more demanding computational efforts but enable the possibility of carrying out predictive parametric analysis regarding the influence of tyre design parameters [7].

On the other hand, experimental investigations can be performed, and specific signal processing techniques can be applied in order to identify the parameters useful for model calibration and NVH analyses. To this aim, different methodologies have been proposed in literature. Natural frequencies, mode shapes and modal damping coefficients can be identified through Experimental Modal Analysis

* Corresponding author.
E-mail address: ivano.lapaglia@polimi.it (I. La Paglia).

https://doi.org/10.1016/j.ymssp.2024.111181
Received 22 June 2023; Received in revised form 20 December 2023; Accepted 23 January 2024

(EMA). This analysis can be performed in static conditions, where the tyre is excited at one location through an impact hammer or a shaker, and accelerations are measured at different positions along the tyre circumference. The Frequency Response Functions (FRFs) of the system are computed and used in the extraction of the modal parameters. Several test bench configurations have been proposed in literature to carry out the EMA of a static tyre, such as in [8,9].

Although tyre vibrations have been deeply studied in static conditions, difficulties arise when dealing with a rolling tyre. At first, vibration measurements cannot be easily performed with conventional accelerometers placed on the tyre outer surface. Therefore, other measuring systems such as laser Doppler vibrometer should be considered [10]. Furthermore, the dynamic response at the contact patch cannot be measured. Secondly, a reliable identification of the input force becomes challenging. This prevents the execution of the classical EMA, and other identification techniques must be considered. In literature, most of the authors rely on the Operational Modal Analysis (OMA) to identify the modal parameters of the rolling tyre [9,11–14].

Regarding the test configuration, one of the typical solutions adopted to excite a rolling tyre in indoor conditions relies on a cleat test, where the tyre rolls over an obstacle providing an impulsive-like excitation. This test is suitable for understanding the tyre low frequency dynamic behaviour, given that the maximum frequency excited by the cleat impact is approximately 300 Hz [2]. For instance, a cleat test was carried out in [15] mounting the obstacle on the surface of a 2 m diameter steel drum, with a perpendicular inclination with respect to the tyre rolling plane. The tyre hub forces were measured and used to tune an in-plane ring model. A similar test setup was used in [9], where a laser Doppler vibrometer was adopted to measure the tyre radial surface vibrations. An alternative cleat test setup was proposed in [13], constituted by two identical tyres which rotate one against the other. The undriven wheel is mounted on a dynamometric hub which allows the measurement of the forces generated during the test. The excitation is provided by an aluminium cleat mounted on the driven wheel, and a laser Doppler vibrometer was used to measure the surface vibrations.

A phenomenon that has been observed by many authors during rolling tyre tests is the bifurcation effect [16]. In static conditions, input forces generate progressive and regressive waves that propagate along the tyre structure at the same speed. Consequently, their superposition results in standing wave vibration modes. In rolling conditions, progressive and regressive waves travel at different propagation speeds due to Coriolis accelerations. Moreover, a Doppler frequency shift is present if the tyre rotation is observed in a fixed reference system. The Coriolis effect prevents the realization of standing waves, and the resulting modes will be complex; thus, they will present a propagation velocity [9,13,16–18]. The bifurcation effect depends on the tyre rolling speed, the considered mode number and the corresponding mode shape. Based on these considerations, the classical definition of mode shape cannot be applied to rotating systems, and identification techniques should be based on wave propagation models.

This paper aims at investigating the in-plane dynamic behaviour of a rolling tyre in the frequency range below 300 Hz through an indoor experimental approach. A measuring setup specifically designed to this purpose is presented. A cleat test is performed on a steel drum, and tyre radial vibration measurements are carried out through a laser triangulation sensor scanning the tread of the rolling tyre. Data are collected at different rolling speeds and inflation pressures to investigate the influence of both parameters on the tyre dynamics. Secondly, starting from the tyre surface vibration at several positions along the tyre circumference, a strategy to identify the wave propagation field is proposed. With respect to previous publications, in this paper experimental data are fitted using a wave propagation formulation. Through this approach, no Complex Modal Testing [19] or Operational Modal Analysis techniques are

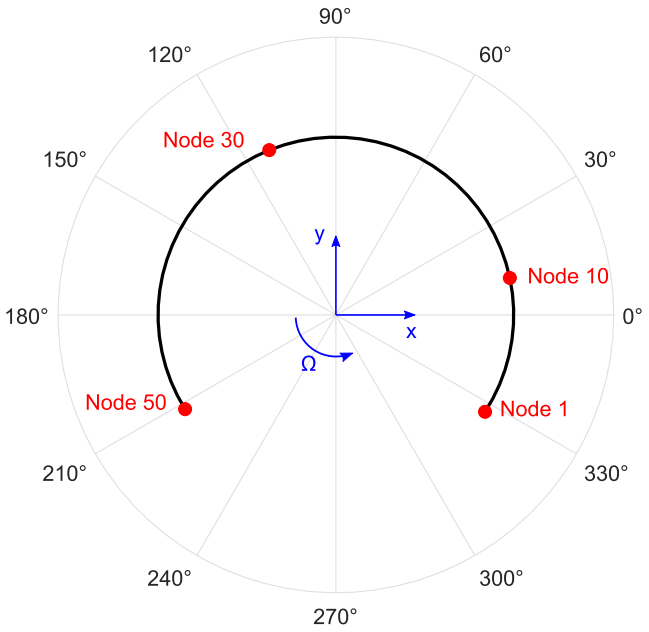

Fig. 1. Measurement grid: 50 nodes regularly spaced every 5°, from –33° to +212° (their position is defined in the fixed reference system). For visualization purposes, only nodes 1, 10, 30 and 50 are highlighted.

applied; no analytical model is involved during the identification procedure, such as in [11,12]. The discontinuity in tyre radial vibration due to the contact patch is taken into account enabling the identification of real circumferential mode numbers. In addition, to interpret the results, the test data have been compared to the analytical results obtained with a simplified in-plane tyre model, showing a satisfactory degree of correlation.

The paper is organized as follows. In Section 2, the experimental setup realized to measure the tyre response during a cleat test is described. In Section 3, the data processing technique to synchronize data and extract the tyre vibration out of the recorded time histories is described; then, the wave propagation algorithm is presented and details on the fitting procedure are provided. In Section 4, different datasets are compared in order to investigate the influence of speed and inflation pressure; in addition, the results are compared with those of a tyre analytical model. Eventually, Section 5 draws the conclusions of this work.

2. Experimental setup

In order to measure the vibration of the tyre in rolling conditions, a dedicated experimental setup has been designed and installed in an existing facility, where cleat tests are carried out. The test rig is made up of a steel drum driven by an electric motor. A laser triangulation sensor (MEL Microelectronics M7L 50) is adopted to scan the tyre surface. The sensor has a measuring range of 50 mm around the focus distance of 95 mm. It is kept at a fixed distance from the tyre by the supporting structure, and it measures the tyre response after the cleat impact. The vibration measurements have been performed at 50 positions (nodes) along the tyre circumference. A measurement grid of 5° has been adopted, with a total covered angle of 245°. Due to the contact patch and the contiguous regions that could not be reached by the laser beam, given the presence of the drum, no measurements could be performed over 115°. For the sake of clarity, Fig. 1 shows the measurement grid: for visualization purposes, only few nodes are reported. The centre of the contact patch is located at the angle position 270°, while the first measuring position is in correspondence of the angle 327°. The blue arrows on Fig. 1 show the adopted convention for the reference system and the tyre rolling direction. In this work, a transversal cleat (perpendicular to the x-y plane) was used, and we refer to radial vibrations occurring in the x-y plane as the in-plane tyre response.

The structure that carries the sensor was designed to be stiff and stable in order to measure the tyre vibration, reducing as much as possible any disturbance. To this end, the structure was installed on supports that are dynamically decoupled from the test rig basement by means of a suspended foundation. Fig. 2 shows a 3D CAD model of the designed system, that is constituted by two set of elements: a fixed rigid frame (supporting structure), which carries the loads and provides the required stiffness; a moving structure connected to the fixed frame, that supports the laser sensor and which can be fixed at different angular positions around the centre of the tyre.

Considering the moving structure, it is positioned at the centre of the horizontal beam, aligned with the centre of the tyre. The rotation of the structure (red dashed line in Fig. 2b) is provided by an electric motor. At each position, the tyre vibration is acquired for 30 s at a sampling frequency of 5 kHz. Once the acquisition is completed, the sensor automatically moves to the subsequent position. To reduce the effect of the oscillations induced by the arm rotation, before to start the next acquisition, further 30 s are considered so as to reach a static condition. At the end of the test, 50 time histories are collected.

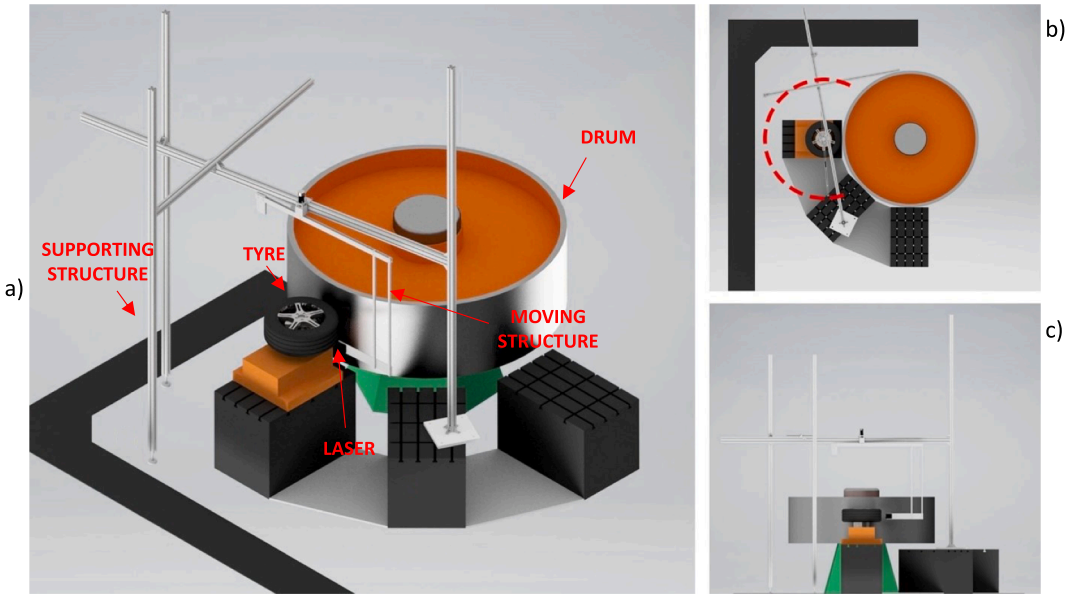

Fig. 2. a) 3D CAD model of the laboratory setup used for the measurements on a rolling tyre. Red dashed line in b) indicates the trajectory followed by the measuring system during operation. c) Side view. (For interpretation of the references to colour in this figure legend, the reader is referred to the web version of this article.)

Fig. 3 shows a picture of the test bench. In Fig. 3a an overview of the designed system is provided, with the tyre loaded against the driving drum; Fig. 3b shows a detail of the laser triangulation sensor together with the cleat (5 mm height, 10 mm length along the rolling direction) adopted to excite the tyre.

3. Vibration measurements on a rolling tyre

In this section, the methodology developed to investigate the dynamic behaviour of the rolling tyre is presented. In Section 3.1, the processing of the time histories collected along the tyre circumference is described; in Section 3.2, the wave field identification algorithm is presented.

3.1. Signal processing

The experimental setup described in Section 2 allowed measuring the tyre radial vibration consequent to the cleat impact. Data have been collected at speeds of 50 and 90 km/h and inflation pressures of 2.2 and 2.7 bar in order to investigate the effects of these changes on the tyre dynamics. Trigger signals of the tyre and drum rotations have been recorded to allow the data synchronization and post-processing. In the following, a single time history (node 50, 212°) out of the 50 available, measured at 50 km/h at a pressure of 2.2 bar, is considered as a reference case to present the experimental results and data processing.

Fig. 4a shows the displacement signal acquired by the laser triangulation sensor for two subsequent impacts. It is possible to notice that the signal is constituted by two main components: the first one, with a time periodicity of 0.15 s, is related to the tyre non-uniformity; the second and most important one is associated to the dynamic response of the tyre due to the cleat impact, and it shows a period of 0.57 s (identified by a vertical dashed line).

In this paper, the analysis is focused on the investigation of the tyre free response due to the cleat excitation. Thus, two signal processing steps are required: on the one hand, the tyre non-uniformity contribution was removed; on the other, the forced response (initial time instants associated to the cleat-tyre interaction) was recognised and discarded from the data.

At first, attention is paid to the tyre non-uniformity contribution. The tyre trigger signal (periodic with the tyre rotation) was used to isolate the time windows associated to every tyre passage. Later, time-averaging was used to generate the non-uniformity signal, for a single tyre revolution. Then, this signal was replicated to have a time history of the same length of the original signal, as shown in Fig. 4b. Finally, the tyre response associated only to the cleat excitation was obtained by subtracting the time histories of Fig. 4a and b. The achieved result can be observed in Fig. 4c.

Once the tyre non-uniformity was removed, the average cleat response was evaluated to limit the influence of background noise. To this end, the drum trigger was used to identify the time windows related to a cleat impact (vertical dashed line in Fig. 4c), and time-domain averaging was applied to a total of 52 cleat responses. Moreover, the signal related to the first order of the drum revolution was removed since this signal component is not related to the cleat response. The result of this procedure is shown in Fig. 5 as a black line.

In addition, the standard deviation of the collection of 52 measurements was quantified to be of approximately 50 μm during the whole drum revolution. This value, associated to the background noise, is significantly smaller compared to the vibration levels shown in Fig. 5. Moreover, the averaging operation further reduces this measurement uncertainty.

The black signal shown in Fig. 5 consists of both the forced response (when the tyre rolls over the obstacle) and the subsequent free response, which is the main focus of this work. Therefore, the next step of the signal processing is the distinction of the two contributions. To this aim, the duration of the cleat impact was estimated, given the size of the obstacle (5 mm height), the contact patch length and the corresponding tyre angular section influenced by the cleat excitation (0.58 rad). An example of the distinction of the time response influenced by the cleat impact (forced response) and the tyre free response can be observed in Fig. 5. Note that the duration of the free response (red curve) was identified considering a thirty-fold amplitude reduction (evaluated considering the whole

Fig. 3. Test bench for vibration measurements on a rolling tyre. a) Overview of the laboratory with tyre installed on the test machine. b) Detailed view of the laser triangulation sensor and the cleat adopted to excite the tyre.

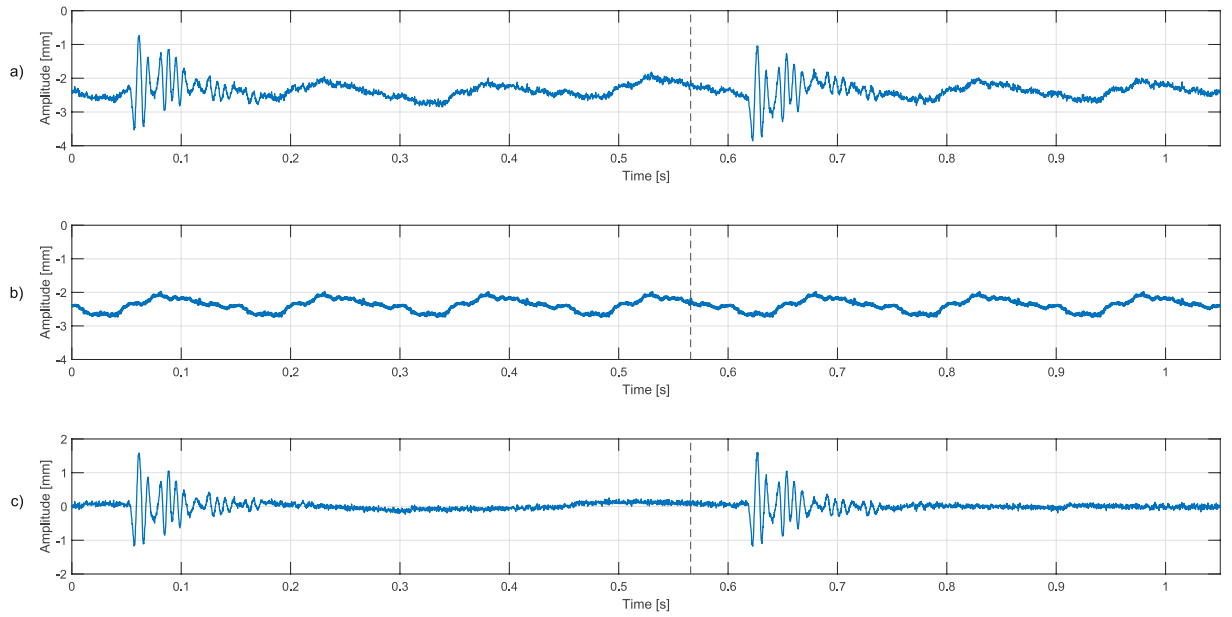

Fig. 4. Laser signal measured at 50 km/h, 2.2 bar, angular position 212° (node 50). a) Measured response to the cleat excitation; b) tyre non-uniformity; c) laser signal with reduced non-uniformity component, obtained as the algebraic subtraction of signals a) and b).

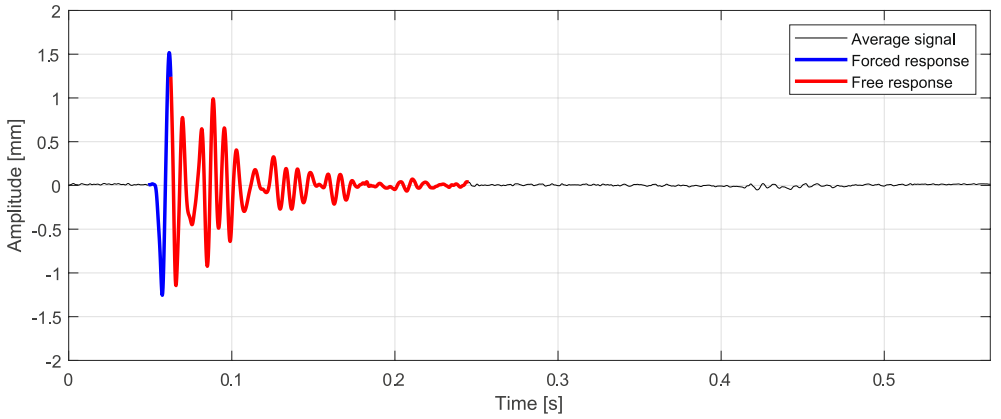

Fig. 5. Distinction of the tyre free and forced response from the average dynamic response (50 km/h, 2.2 bar, node 50, angular position 212°).

measurement grid). This was necessary to limit the amount of data to be later processed, still ensuring to include all the relevant harmonic contributions of the tyre free response.

Finally, the described procedure was iterated for all 50 angular positions. In doing so, the tyre trigger signal allowed to synchronize all the measured time histories.

3.2. *Wave field identification algorithm*

In this section, the algorithm adopted to identify the dynamic behaviour of the tested tyre is presented. The collected experimental signals are fitted through the following model:

$$u_r(\theta,t)=\sum_{i=1}^{n}A_i e^{-\alpha_i t}\cos(\omega_i t-k_i\theta+\phi_i) \tag{1}$$

Eq. (1) represents the tyre free response to the cleat impact, described in the fixed reference system, in terms of radial displacement of the tyre belt u_r. Thus, u_r is defined as a function of both angular position θ and time t. Eq. (1) relies on a wave propagation solution, that models the tyre response as the superposition of both progressive and regressive waves travelling along the tyre circumference. In Eq. (1):

- u_r is defined as the summation of n travelling waves, n being an even number associated to the order of the system (defined a priori, as later addressed) and $n/2$ representing the number of progressive and regressive wave pairs propagating along the tyre circumference;
- $\omega_i = 2\pi f_i$ is the circular frequency of the i-th wave function;
- k_i represents the circumferential mode number, that is a real constant assuming positive values in case of progressive waves (travelling counterclockwise, in the same direction as the tyre rotation) and negative values in case of regressive waves (travelling clockwise, against the tyre rotation);
- A_i and ϕ_i are real constants respectively associated to the amplitude and the phase of the generic i-th wave;
- α_i is the damping coefficient; the damping contribution is represented by the decaying exponential function $e^{-\alpha_i t}$, where $\alpha_i = \xi_i \omega_i$ and ξ_i is the nondimensional damping ratio.

Eq. (1) is evaluated for specific θ values corresponding to the measurement grid of Fig. 1. As a result, for each angular position θ, u_r is a function of time t only. Considering the data collected during the experimental cleat test, the difference between the measured signal and the fitting function of Eq. (1) can be evaluated. At any time instant t and each measurement position, the squared error has been evaluated and the cost function to be minimized has been defined based on the cumulated error. In order to identify the unknown parameters of Eq. (1), a nonlinear data fitting has been performed by means of the *lsqnonlin* Matlab function.

Although all the $5xn$ parameters are identified at the end of the minimization procedure, attention should be focused on the values of the circumferential mode number k. When the case of the unload tyre is considered, the circumferential mode number k needs to be an integer [17]. In fact, since the tyre is closed in the θ direction and no constraints are applied on the tread surface, the period of the function u_r is necessarily an integer submultiple of 2π. However, in the considered case, the tyre is loaded against the drum, and therefore some influence of the contact patch is expected. Consequently, no constraints on the parameter k have been imposed, leaving it free to assume any real value.

In order to find the global minimum of the error function, the *lsqnonlin* function requires reliable initial values for the parameters. These have been estimated by analysing the 2D Fast Fourier Transform (2D FFT) of the available time histories. Fig. 6a shows the results of the 2D FFT processing applied to the reference dataset (50 km/h, 2.2 bar). The x and y axes respectively report the circumferential mode number and the frequency of the wave contributions. The zero-padding technique was adopted to manage the data measured along the tyre portion of 245°, to increase the spatial resolution in terms of circumferential mode numbers k. As a result, it can be observed that integer circumferential mode numbers k are obtained. It is worth clarifying that this strategy was used just to compute the initial values for the minimization. Conversely, at the end of the minimization, the k values are expected to assume non-integer values, as also confirmed in [12].

Attention is now paid to the estimation of the initial guesses. Fig. 6a allows estimating the number of waves mainly contributing to the overall tyre free response. Five progressive and five regressive waves are mostly highlighted in the colormap, thus defining the n parameter of Eq. (1) for the considered dataset (50 km/h). Note that n generally varies depending on the tyre speed.

Reference is now made to a specific column of the Fig. 6a, which represents the spectrum of the signal for fixed circumferential mode number (i.e., for every wave function). For instance, Fig. 6b shows the harmonic content associated to $k_i = -2$. The spectrum allows estimating first attempt values for the amplitude A_i, extracted considering the most relevant harmonic component, and the

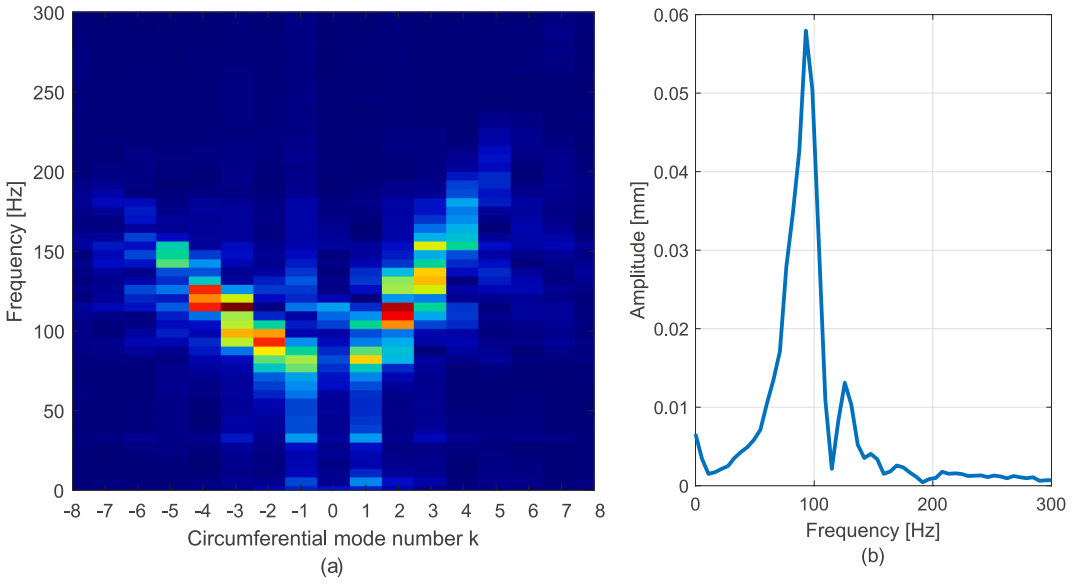

Fig. 6. Signal processing for the initial guess estimation (reference dataset 50 km/h, 2.2 bar). a) results of the 2D FFT processing; b) spectrum associated with the $k = -2$ wave function.

corresponding frequency ω_i. The nondimensional damping ratio ξ_i was estimated according to the half-power point method. Finally, the phase ϕ_i was set to a null value as first attempt guess.

4. Results and discussion

In this section, the outcomes of the identification process are presented and discussed to investigate the effect of tyre rolling speed and inflation pressure. At first, a reference case is analysed, with the tyre inflated at 2.2 bar and rolling at 50 km/h. The identified model parameters are listed in Table 1, with each column associated with a specific parameter. Progressive and regressive waves are considered separately and listed for increasing values of the circumferential mode number k. As expected, the k values are not integer numbers. However, it is generally possible to identify pairs of circumferential mode number with positive and negative values, and similar magnitude, although the corresponding frequencies are considerably different (this observation will be later analysed in more detail in Fig. 12). These results are in general accordance with those reported in [12].

The quality of the identification can be checked by plotting the identified wave function superimposed to the experimental signal. For instance, Fig. 7 shows the comparison between the identified signals and the experimental ones, corresponding to the measurement nodes 10 and 30. The same procedure can be applied to each one of the 50 measuring positions. The vertical dashed lines in Fig. 7 identify six time instants (the first occurring at t = 0 s) that will be later considered in Fig. 9.

A satisfactory degree of agreement is reached between the experimental and identified free response, respectively shown as a solid red line and a dashed black one.

For the sake of completeness, Fig. 8 shows the mean square error computed over the whole duration of the free response for each of the 50 measuring positions.

Slightly worse performances are observed in proximity of the contact patch. As a result, an increase in the identification error can be recognised for these measurement positions. This is related to slight mismatch of the signal amplitudes at these locations during the initial portion of the time history.

Table 1
Results of the identification procedure. Reference case: tyre speed of 50 km/h, inflation pressure of 2.2 bar. Influence of rolling speed: tyre speed of 90 km/h, inflation pressure of 2.2 bar. Influence of inflation pressure: tyre speed of 50 km/h, inflation pressure of 2.7 bar.

Reference case:		k	f [Hz]	ξ [%]	A [mm]	ϕ [rad]
50 km/h, 2.2 bar	**Regressive**	−5.06	149.20	2.41	0.22	−1.49
	waves	−3.99	125.81	2.89	0.27	−2.18
	(clockwise)	−3.38	115.01	2.38	0.33	−1.36
		−2.42	95.59	4.12	0.40	−2.62
		−1.25	80.23	12.10	0.53	−0.55
	Progressive	1.19	82.97	6.35	0.34	1.25
	waves	2.03	110.29	3.82	0.46	1.61
	(counterclockwise)	2.72	132.08	3.29	0.32	−1.36
		3.32	154.96	3.59	0.37	−1.51
		4.07	185.57	4.33	0.26	−2.00
Influence of rolling speed:		k	f [Hz]	ξ [%]	A [mm]	ϕ [rad]
90 km/h, 2.2 bar	**Regressive**	−6.17	148.17	3.40	0.29	1.05
	waves	−5.54	136.88	4.18	0.36	−0.32
	(clockwise)	−4.36	118.63	2.27	0.21	−1.06
		−3.67	107.90	2.74	0.42	−2.80
		−3.02	96.61	4.08	0.25	2.05
		−2.23	87.60	4.45	0.27	−1.42
		−1.33	76.36	6.24	0.43	−2.13
	Progressive	1.14	82.44	10.61	0.55	−0.71
	waves	2.12	122.47	7.98	0.74	−0.90
	(counterclockwise)	3.06	164.97	6.41	0.70	−1.15
		4.10	210.02	4.62	0.51	−1.05
		5.05	252.00	3.51	0.35	−0.97
		5.91	292.80	3.13	0.24	−1.04
		6.76	329.36	2.77	0.12	−1.14
Influence of inflation pressure:		k	f [Hz]	ξ [%]	A [mm]	ϕ [rad]
50 km/h, 2.7 bar	**Regressive**	−5.02	157.54	2.92	0.22	−0.39
	waves	−3.92	134.28	2.14	0.20	−1.39
	(clockwise)	−3.46	123.11	2.35	0.29	1.92
		−2.42	101.74	4.16	0.42	0.84
		−1.08	81.93	15.52	0.54	0.07
	Progressive	1.16	87.38	5.82	0.30	−1.68
	waves	2.17	117.39	4.30	0.49	−0.89
	(counterclockwise)	2.93	144.64	3.85	0.34	−1.13
		3.54	165.06	2.08	0.17	−0.55
		4.14	193.74	4.80	0.19	−1.31

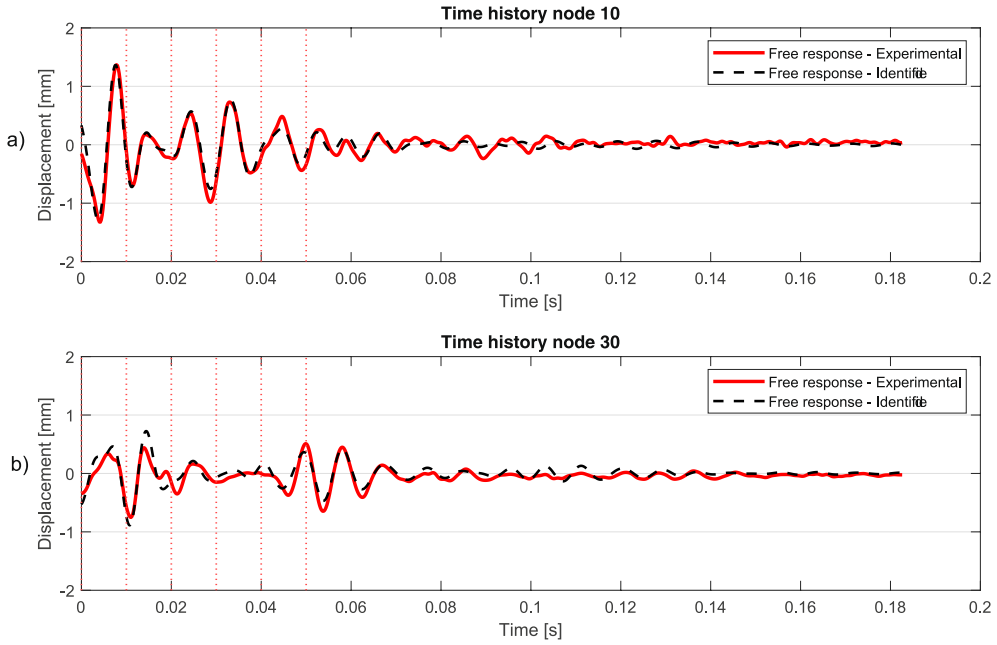

Fig. 7. Comparison of the experimental and identified time histories of the free response of a) node 10; b) node 30. Tyre speed of 50 km/h, inflation pressure of 2.2 bar.

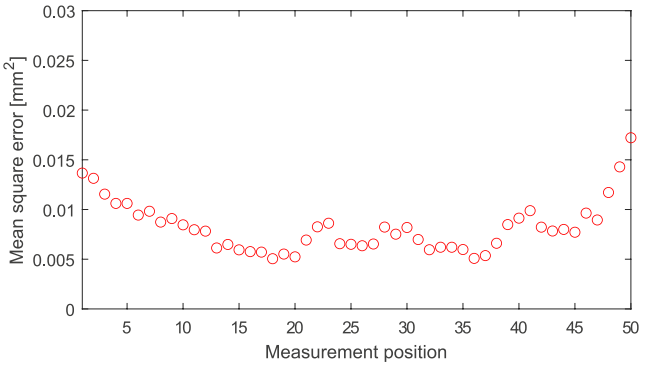

Fig. 8. Mean square error between the experimental and identified signals as a function of the measuring position. Tyre speed of 50 km/h, inflation pressure of 2.2 bar.

Finally, in Fig. 9 the tyre deformed configurations about the mean radius at different time instants of the free response are presented: the red solid curves stand for the experimental signal, while the identified signals are reported as black dashed lines. For simplicity, the tyre rolling direction is also reported as a blue arrow. The red dots identify nodes 10 and 30, whose time histories were presented and discussed in Fig. 7. Good correspondence can be observed between the two signals at most of the instants and angular positions, meaning that the algorithm provides reliable results to identify the free response of the rolling tyre. Minor amplitude mismatches are visible at the inlet and outlet regions at the initial time instants, confirming the considerations drawn from Fig. 8.

The analysis can be extended to other dataset in order to verify the effectiveness of the algorithm. To this end, the influence of speed (experimental data gathered at 90 km/h at the same inflation pressure of 2.2 bar) and of pressure (considering an inflation pressure of 2.7 bar at the nominal speed of 50 km/h) will be analysed in the following sections.

To summarize the results of the identification procedure, Table 1 lists all the parameters for the considered test cases, distinguishing between the reference case (50 km/h, 2.2 bar), the dataset adopted to investigate the influence of the rolling speed (90 km/h, 2.2 bar) and of the inflation pressure (50 km/h, 2.7 bar) on the tyre dynamics.

4.1. Influence of rolling speed

Considering the data collected at a higher speed of 90 km/h, the propagation of the waves on the tyre surface will be different with respect to the previous case. Given the higher speed, the obstacle impact will excite a higher number of waves, so that 14 contributions

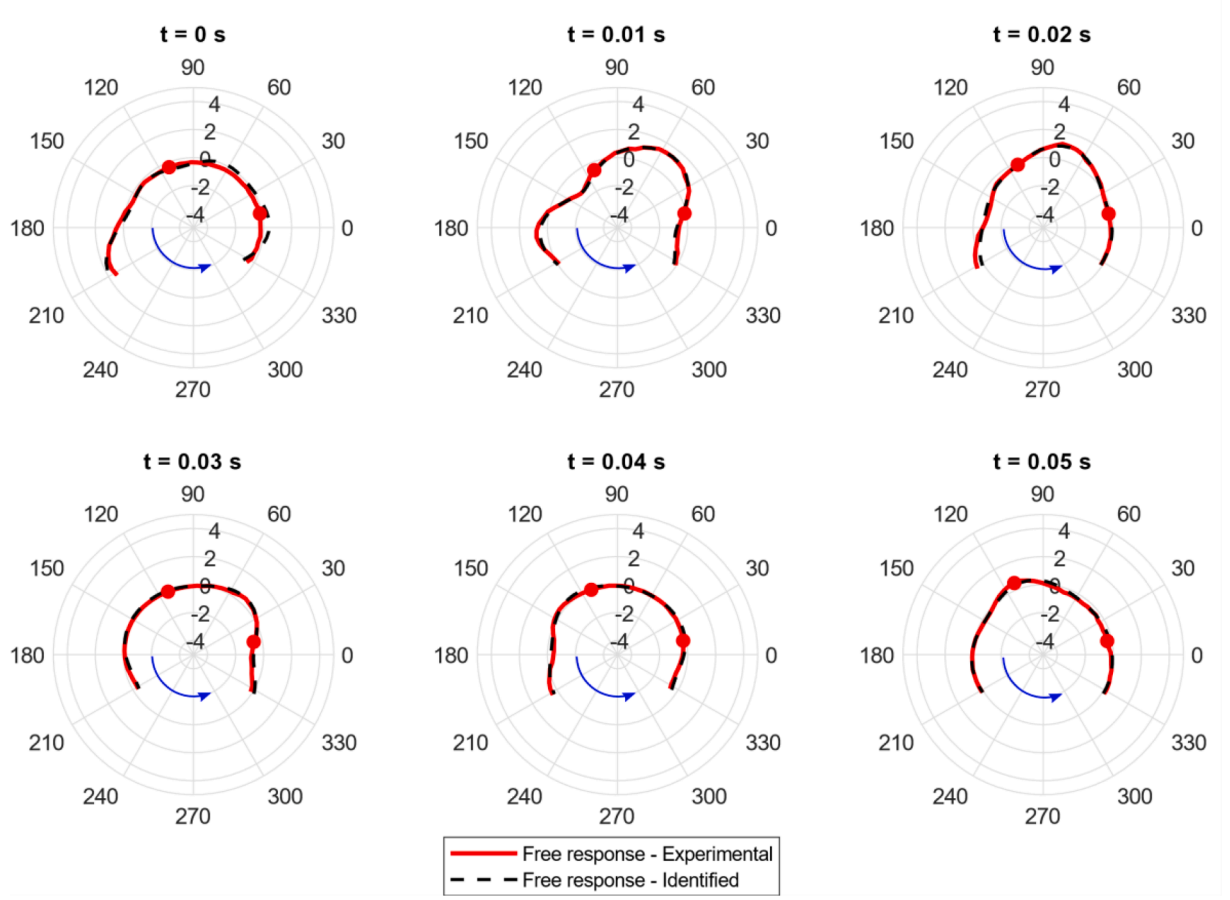

Fig. 9. Comparison of the experimental and identified tyre deformation at different time instants of the free response. Tyre speed of 50 km/h (42 rad/s), inflation pressure of 2.2 bar.

(thus, $n = 14$ in Eq. (1) evenly split between progressive and regressive waves have been considered. The outcomes of the identification procedure are reported in Table 1. Regarding the identification error, the results show a trend similar to the one presented in Fig. 8.

The comparison between the measured and identified tyre free responses is shown in Fig. 10. Specifically, in Fig. 10a the results are presented in terms of time histories in correspondence of the measuring position denoted as nodes 10. Three time instants are identified by vertical red lines, for which the comparison of the measured and identified tyre deformation is presented in Fig. 10b. The proposed modelling approach proves to be effective, being the red solid and black dashed curves in good agreement at any time instant. If reference is made to Fig. 10b, also the tyre deformation confirms the model capability to reproduce the dynamic response of the whole tyre to the cleat excitation.

The increase of rolling speed causes several variations of the identified parameters with respect to the reference case. Considering Fig. 10a, higher vibration levels (up to 2 mm) are reached compared to those measured at a rolling speed of 50 km/h (see Fig. 7). Higher vibrations are visible also throughout the other measurement positions. From an identification point of view, the amplitudes of the progressive waves show higher values, whereas no clear trend can be extrapolated from regressive waves. The overall higher amplitude of vibration is justified also by the higher number of identified contributions, meaning that most of the signal energy is spread over a higher number of propagating waves ($n = 14$).

Moreover, the effect of rolling speed is related the well-known bifurcation effect [9,13,16–18]. The increase of the tyre rolling speed modifies the waves propagation, causing progressive waves to be faster and regressive waves to be slower. For the test case under analysis, this can be confirmed by computing the ratio between the frequency f_i of each wave and the circumferential mode numbers k_i. The results are shown in Fig. 12 as dispersion diagram ($k_i - f_i$ plot).

Focusing on the identified k_i and f_i values, they are both affected by the rolling speed. The identification results show that at higher speed, in general, both quantities increase for progressive waves and decrease for regressive waves. It can be concluded that the waves frequency f_i changes more than k_i when the rolling speed changes.

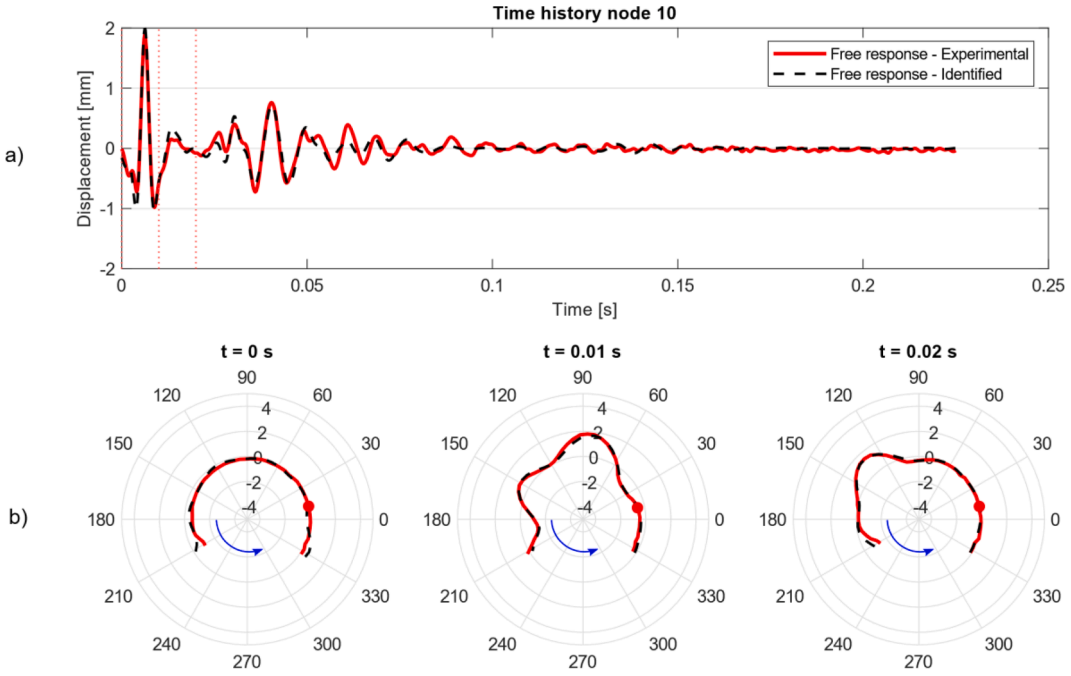

Fig. 10. Comparison of the experimental and identified results, considering the tyre speed of 90 km/h (76 rad/s) and inflation pressure of 2.2 bar. a) Comparison of the time histories of the free response for node 10. b) Comparison of the tyre deformation at different time instants of the free response.

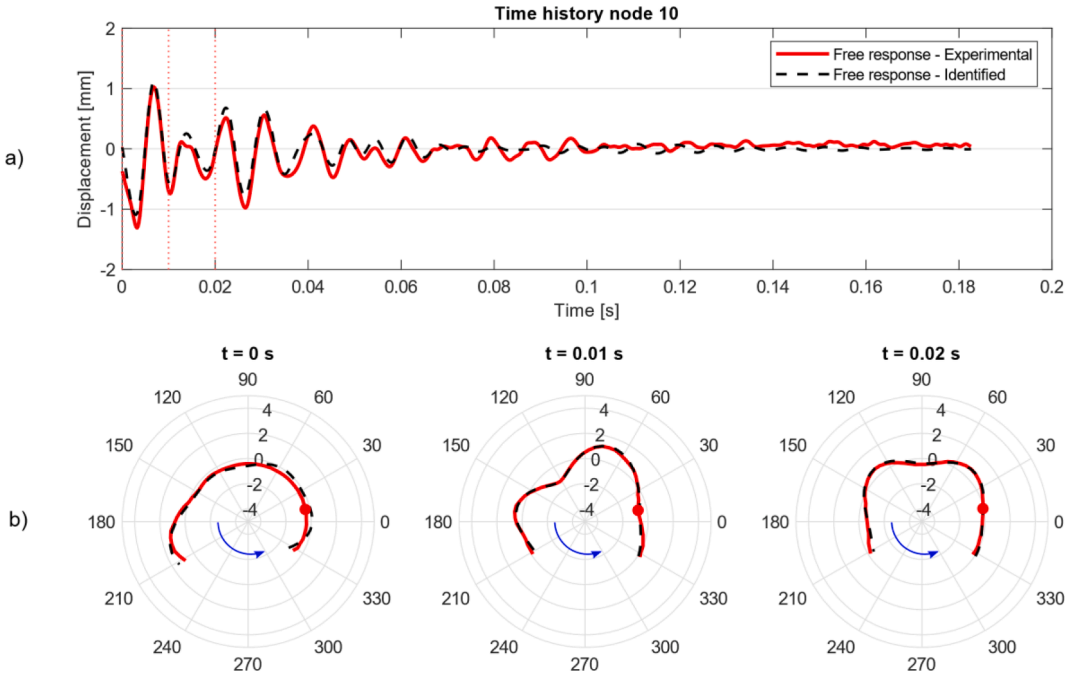

Fig. 11. Comparison of the experimental and identified results, considering the tyre speed of 50 km/h (42 rad/s) and inflation pressure of 2.7 bar. a) Comparison of the time histories of the free response for node 10. b) Comparison of the tyre deformation at different time instants of the free response.

4.2. Influence of inflation pressure

As a second analysis, data gathered at 50 km/h at a higher inflation pressure of 2.7 bar are considered. The identification procedure relies on the same steps adopted at 2.2 bar, thus including the contribution of $n = 10$ travelling waves to the tyre free response. The time domain comparison between the signals measured by the laser and those identified by the model is proposed in Fig. 11. In Fig. 11a the comparison is carried out considering the time histories of node 10, whilst in Fig. 11b the animation of the tyre deformation is shown. A significant degree of agreement can be recognised comparing the measured and the identified tyre vibration, both in terms of amplitudes and frequency components.

The influence of the inflation pressure on the dynamics is driven by changes of the tension of the tyre reinforcements, which increases at higher pressures [2]. Therefore, a stiffening effect is observed, which causes waves to propagate at higher speed. This is mainly visible as an increment of the wave frequencies, for both progressive and regressive waves. For the test case under analysis, an average variation of +6 % is observed. Slight modifications of the circumferential mode numbers can be observed too, but no clear trend can be extrapolated from the identified data. It is worth mentioning that the modifications of the circumferential mode numbers might be related to changes in the footprint dimensions due to the different inflation pressure.

4.3. Comparison with in-plane tyre flexible ring model

In this section, the relationship between the k and f values identified by the proposed methodology is compared with the results of a simplified in-plane flexible ring tyre model. The model is presented in [17], and its parameters have been tuned based on an Experimental Modal Analysis carried out on the same tyre considered in this manuscript. The considered analytical model, although simplified and reproducing an unloaded rotating tyre, was chosen since it directly allows evaluating the dispersion curve of the rotating tyre [16,20]. This can be regarded as a major advantage compared to other modelling strategies. For instance, Finite Element Models would allow computing the natural frequencies and mode shapes, but it would not be possible to directly derive the corresponding circumferential mode number.

The comparison between the identified and analytical results has been performed considering different inflation pressures and tyre rotating speeds, to match the experimental data. The results are reported in Fig. 12 in terms of dispersion diagrams, showing the circumferential mode number k along the x-axis and the frequency f of the considered wave contribution along the y-axis. It is remined that the tyre is rolling in counterclockwise direction, and that waves characterized by positive k values rotate together with the tyre, while negative k values are associated to clockwise travelling direction. It is worth noting that while real circumferential mode number k are considered in this paper (reported as dot markers), integer values are adopted by the analytical model (reported as dashed lines with cross markers). This difference is consistent with the tyre conditions adopted in the two cases: when the tyre is rolling during the experimental cleat test, the contact patch introduces a discontinuity in the wave field propagating along the tyre belt. Conversely, the analytical results of the simplified model consider a rotating tyre (unloaded tyre, no contact patch).

Despite the differences in terms of tyre conditions (loaded and unloaded), the comparison shown in Fig. 12 allows observing that the (k_i, f_i) couples experimentally identified (reported as dots) are respecting the trend of the analytical rotating flexible ring (dashed lines with cross markers), both in case of rolling speed (Fig. 12a) and inflation pressure (Fig. 12b) increase.

Focussing on the effect of tyre speed, Fig. 12a shows that an increase in the rolling speed leads to an increase in the frequency of the waves characterized by positive circumferential mode numbers. Conversely, waves with negative circumferential mode number are subjected to a decrease in the frequency. This behaviour can be related to the well-known bifurcation effect observed in a fixed reference frame [17]. If reference in now made to the effect of the inflation pressure, Fig. 12b shows an average increase of the frequencies of +6 %, which is particularly visible at higher circumferential mode numbers. This behaviour is characteristic of both progressive and regressive waves, that is associated to the tyre structure stiffening effect. Some differences can be recognised, for instance in Fig. 12a on the branch representing the positive k values, that can be associated to the uncertainties associated to the experimental data and to the simplifying assumptions of the analytical model.

The comparison between the experimental data for the loaded tyre and the analytical model predictions for the unloaded tyre shows that the operating conditions have a minor effect on the relationship between k and f.

5. Conclusions

This paper aims at investigating the in-plane dynamic behaviour of a rolling tyre in the frequency range below 300 Hz. To this end, at first the rolling tyre response to the cleat impact has been experimentally characterized. The measuring setup specifically designed to this purpose has been described. It relies on a completely automated system, constituted by a fixed and a moving structure which carries a laser triangulation sensor. The system allows scanning the tyre radial vibration after the cleat impact, along a predetermined measurement grid of 5°. Experimental data have been gathered at different rolling speeds and inflation pressures, so as to investigate the influence of both parameters on the tyre dynamics.

Secondly, a data processing algorithm to identify the travelling waves that contribute to the response of the tyre has been presented. The model relies on a wave propagation solution, and it purposely allows considering real circumferential mode numbers on account of the contact patch, that introduces a discontinuity in the tyre vibration. A significant agreement between the measured and identified signals has been achieved, both in terms of time histories (at a fixed position along the tyre circumference) and of dynamic deformation. The performance of the identification algorithm has been tested considering experimental data collected at different rolling speeds and inflation pressures.

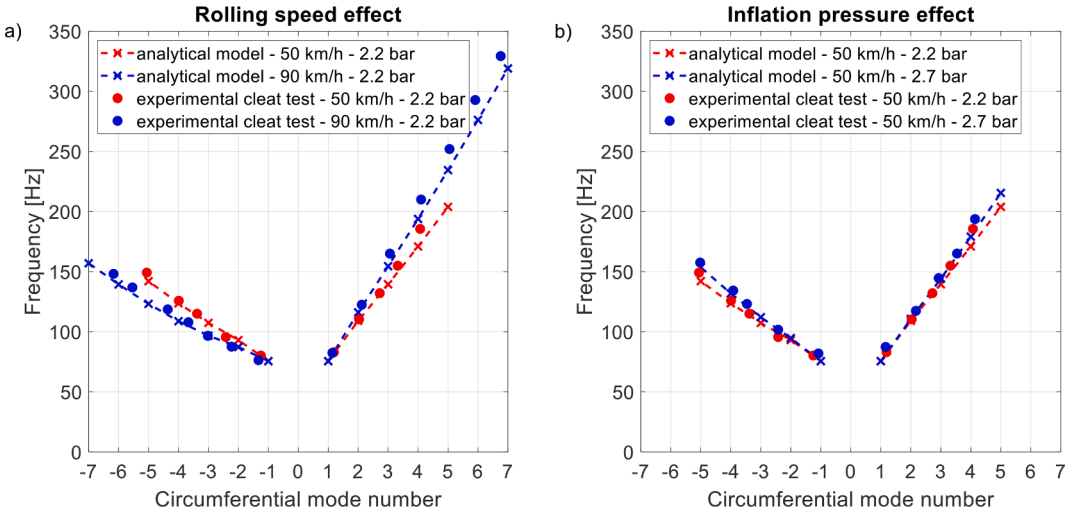

Fig. 12. Dispersion diagrams comparing the identified results with those achieved with an in-plane tyre flexible ring model, considering the fixed reference frame. a) Influence of rolling speed; b) influence of inflation pressure.

Finally, the identified data have been compared with the analytical results obtained with a simplified in-plane tyre model, showing a satisfactory degree of agreement. Both the bifurcation effect related to the speed increase and the stiffening effect related to the pressure increase are well observed and replicated. In addition, the comparison suggests a minor effect of the tyre loading conditions on the dispersion diagrams.

In the end, the designed measurement system and wave field identification algorithm may represent useful tools to investigate the dynamic behaviour of the rolling tyre, to possibly support the product development and to mitigate structure-borne noise contribution.

CRediT authorship contribution statement

Ivano La Paglia: Conceptualization, Methodology, Writing – original draft, Validation. **Luca Rapino:** Conceptualization, Methodology, Validation, Writing – original draft. **Francesco Ripamonti:** Formal analysis, Methodology, Supervision, Validation, Writing – review & editing. **Simone Baro:** Resources, Validation, Visualization. **Roberto Corradi:** Funding acquisition, Project administration, Supervision, Writing – review & editing.

Declaration of competing interest

The authors declare that they have no known competing financial interests or personal relationships that could have appeared to influence the work reported in this paper.

Data availability

The data that has been used is confidential.

Acknowledgments

This study is part of the Structure Borne Tyre Noise (SBN), carried out in the framework of the Joint Labs cooperation agreement between Politecnico di Milano and Pirelli. The authors gratefully acknowledge Pirelli for providing the support and data necessary to this work.

Funding

This research did not receive any specific grant from funding agencies in the public, commercial, or not-for-profit sectors.

References

[1] U. Sandberg, J.A. Ejsmont, Tyre/road Noise Reference Book, INFORMEX, 2002.
[2] X. Wang, Automotive Tire Noise and Vibrations, Elsevier, 2020. doi: 10.1016/C2018-0-02431-7.
[3] H. Huang, X. Huang, W. Ding, M. Yang, D. Fan, J. Pang, Uncertainty optimization of pure electric vehicle interior tire/road noise comfort based on data-driven, Mech. Syst. Sig. Process. 165 (2022), https://doi.org/10.1016/j.ymssp.2021.108300.

[4] M. Constant, J. Leyssens, F. Penne, R. Freymann, Tire and Car Contribution and Interaction to Low Frequency Interior Noise, in: 2001. doi: 10.4271/2001-01-1528.
[5] D. de Klerk, A. Ossipov, Operational transfer path analysis: Theory, guidelines and tire noise application, Mech. Syst. Sig. Process. (2010) 1950–1962, https://doi.org/10.1016/j.ymssp.2010.05.009.
[6] T. Li, R. Burdisso, C. Sandu, Literature review of models on tire-pavement interaction noise, J. Sound Vib. 420 (2018) 357–445, https://doi.org/10.1016/j.jsv.2018.01.026.
[7] H. Nakashima, J.Y. Wong, A three-dimensional tire model by the finite element method, J. Terramech. 30 (1993) 21–34, https://doi.org/10.1016/0022-4898(93)90028-V.
[8] K. Patil, M. Behroozi, J. Baqersad, Experimental modal analysis on a tyre - lessons learned, Int. J. Veh. Noise Vib. 13 (2017) 200, https://doi.org/10.1504/IJVNV.2017.10010555.
[9] C. Gonzalez Diaz, P. Kindt, J. Middelberg, S. Vercammen, C. Thiry, R. Close, J. Leyssens, Dynamic behaviour of a rolling tyre: experimental and numerical analyses, J. Sound Vib. 364 (2016) 147–164, https://doi.org/10.1016/j.jsv.2015.11.025.
[10] P. Castellini, M. Ballatore, How to measure actual tire shape in the rolling condition using Scanning LDV, Mech. Syst. Sig. Process. 24 (2010) 736–745, https://doi.org/10.1016/j.ymssp.2009.09.008.
[11] J. Lee, S. Wang, B. Pluymers, W. Desmet, P. Kindt, A modified complex modal testing technique for a rotating tire with a flexible ring model, Mech. Syst. Sig. Process. 60 (2015) 604–618, https://doi.org/10.1016/j.ymssp.2014.12.002.
[12] J. Lee, S. Wang, P. Kindt, B. Pluymers, W. Desmet, Identification of the direction and value of the wave length of each mode for a rotating tire using the phase difference method, Mech. Syst. Sig. Process. 68–69 (2016) 292–301, https://doi.org/10.1016/j.ymssp.2015.07.003.
[13] P. Kindt, D. Berckmans, F. de Coninck, P. Sas, W. Desmet, Experimental analysis of the structure-borne tyre/road noise due to road discontinuities, Mech. Syst. Sig. Process. 23 (2009) 2557–2574, https://doi.org/10.1016/j.ymssp.2009.04.005.
[14] S. Palanivelu, K.V. Narasimha Rao, K.K. Ramarathnam, Determination of rolling tyre modal parameters using finite element techniques and operational modal analysis, Mech. Syst. Sig. Process. 64–65 (2015) 385–402, https://doi.org/10.1016/j.ymssp.2015.04.006.
[15] Z. Liu, F. Wang, Z. Cai, Y. Wei, S. Marburg, A novel theoretical model of tire in-plane dynamics on uneven roads and its experimental validation, Mech. Syst. Sig. Process. 186 (2023) 109854, https://doi.org/10.1016/j.ymssp.2022.109854.
[16] I. Lopez Arteaga, R.E.A. Blom, N.B. Roozen, H. Nijmeijer, Modelling vibrations on deformed rolling tyres-a modal approach, J. Sound Vib. 307 (2007) 481–494, https://doi.org/10.1016/j.jsv.2007.05.056.
[17] T. Simon, I. la Paglia, F. Ripamonti, R. Corradi, S. Baro, A theoretical model for investigating the structural dynamics of a rolling tyre, J. Comput. Nonlinear Dyn. 17 (2022), https://doi.org/10.1115/1.4053935.
[18] I. la Paglia, L. Rapino, F. Ripamonti, R. Corradi, S. Baro, An in-plane flexible ring model for the analysis of the free and forced response of a rolling tyre. In: Internoise 2022–51st International Congress and Exposition on Noise Control Engineering, 2022, https://doi.org/10.3397/IN_2022_0745.
[19] C.-W. Lee, A complex modal testing theory for rotating machinery, Mech. Syst. Sig. Process. 5 (1991) 119–137, https://doi.org/10.1016/0888-3270(91)90019-2.
[20] S.C. Huang, W. Soedel, Effect of Coriolis acceleration on the free and forced in-plane vibrations of rotating rings on elastic foundation, J. Sound Vib. 115 (2) (1987) 253–274, https://doi.org/10.1016/0022-460X(87)90471-8.